Developmental Cell
Article

A Small Molecule Inhibitor of Redox-Regulated Protein Translocation into Mitochondria

Deepa V. Dabir,[1] Samuel A. Hasson,[1,6] Kiyoko Setoguchi,[2] Meghan E. Johnson,[1] Piriya Wongkongkathep,[1] Colin J. Douglas,[1] Johannes Zimmerman,[1,7] Robert Damoiseaux,[3] Michael A. Teitell,[2,4,5] and Carla M. Koehler[1,4,5,*]
[1]Department of Chemistry and Biochemistry
[2]Department of Pathology and Laboratory Medicine
[3]Molecular Screening Shared Resource
[4]Molecular Biology Institute
[5]Jonsson Comprehensive Cancer Center and Broad Stem Cell Research Center
UCLA, Los Angeles, CA 90095, USA
[6]Present address: National Institute of Neurological Disorders and Stroke, Building 35, Room 2C1014, 35 Convent Drive, Bethesda, MD 20815, USA
[7]Present address: Charité Medical School, 10117 Berlin, Germany
*Correspondence: koehler@chem.ucla.edu
http://dx.doi.org/10.1016/j.devcel.2013.03.006

SUMMARY

The mitochondrial disulfide relay system of Mia40 and Erv1/ALR facilitates import of the small *t*ranslocase of the *i*nner *m*embrane (Tim) proteins and cysteine-rich proteins. A chemical screen identified small molecules that inhibit Erv1 oxidase activity, thereby facilitating dissection of the disulfide relay system in yeast and vertebrate mitochondria. One molecule, *mito*chondrial protein import *blo*ckers from the *C*arla *K*oehler laboratory (MitoBloCK-6), attenuated the import of Erv1 substrates into yeast mitochondria and inhibited oxidation of Tim13 and Cmc1 in in vitro reconstitution assays. In addition, MitoBloCK-6 revealed an unexpected role for Erv1 in the carrier import pathway, namely transferring substrates from the translocase of the outer membrane complex onto the small Tim complexes. Cardiac development was impaired in MitoBloCK-6-exposed zebrafish embryos. Finally, MitoBloCK-6 induced apoptosis via cytochrome *c* release in human embryonic stem cells (hESCs) but not in differentiated cells, suggesting an important role for ALR in hESC homeostasis.

INTRODUCTION

The mitochondrion has translocons of the outer membrane (TOM) and inner membrane (TIM) to import proteins from the cytosol. Proteins with a typical N-terminal targeting sequence are imported via the TIM23 pathway, whereas polytopic inner membrane proteins use the TIM22 import pathway (Chacinska et al., 2009; Mokranjac and Neupert, 2009). In contrast, most of the proteins imported into the intermembrane space (IMS) lack a mitochondrial targeting sequence and employ diverse routes for mitochondrial import (Herrmann and Hell, 2005).

A recently identified pathway in the IMS mediates oxidation of imported proteins that require disulfide bonds to acquire their native conformation (Deponte and Hell, 2009; Koehler and Tienson, 2009; Riemer et al., 2011; Sideris and Tokatlidis, 2010), such as the small Tim proteins and proteins with a twin CX_9C motif (Cavallaro, 2010). In the small Tim proteins, the proximal N-terminal cysteine residues serve as internal targeting sequences that are recognized by the IMS oxidoreductase Mia40 (Milenkovic et al., 2009; Sideris et al., 2009), which functions as a receptor to mediate translocation across the outer membrane (Chacinska et al., 2004). Mia40 contains a redox-active cysteine pair that is maintained in an oxidized state by the sulfhydryl oxidase Erv1 (Tienson et al., 2009). As the imported protein substrate is oxidized, electrons are passed from Mia40 to Erv1, followed by transfer to molecular oxygen or cytochrome *c* (cyt *c*) (Bien et al., 2010; Dabir et al., 2007). Subsequently, cyt *c* can be reoxidized by cyt *c* oxidase of the respiratory chain (Bien et al., 2010) or by cyt *c* peroxidase (Dabir et al., 2007). Thus, Mia40 and Erv1 constitute a mitochondrial disulfide relay system that is also evolutionarily conserved.

Erv1 belongs to the Erv/ALR sulfhydryl oxidase family, and homologous proteins are found in the endoplasmic reticulum (Erv2) of yeast, in the extracellular environment (Quiescin sulfhydryl oxidase), and in the poxvirus family (E10R) (Gerber et al., 2001; Senkevich et al., 2002; Thorpe et al., 2002). In addition to protein translocation, the role of Erv1 in various cellular pathways is exemplified by a number of defects observed in cells that lack functional Erv1 protein. For example, Erv1 is required for the maturation of cytosolic iron-sulfur cluster-containing proteins (Lange et al., 2001). In *erv1* mutant yeast, heme maturation is impaired (Dabir et al., 2007). Also, mutations in mammalian Erv1 homolog, ALR, result in an autosomal-recessive myopathy (Di Fonzo et al., 2009), and ALR has an essential prosurvival role in the maintenance of murine embryonic stem cells (Todd et al., 2010b) and in the regeneration of *Drosophila* imaginal discs (McClure et al., 2008).

Erv1 has several key functions in the IMS, necessitating the characterization of its homolog, ALR, to uncover basic mechanisms in mitochondrial assembly in vertebrate systems. Because Erv1 donates electrons to cyt *c*, Erv1/ALR may have a central

role in apoptotic pathways that lead to cyt *c* release (Dabir et al., 2007). Classically, mitochondrial protein import has been studied using yeast genetics and biochemical assays. However, new approaches are needed to elucidate disease mechanisms and dissect essential functions in mammalian cells. Here, we report a small molecule screening approach to identify Erv1 inhibitors, with the goal of developing a set of probes that can modulate the pathway quickly and recapitulate disease phenotypes. We have taken advantage of the previously developed in vitro Amplex Red assay for monitoring Erv1 activity to identify inhibitors (Dabir et al., 2007). Our results indicate that the small drug-like inhibitor characterized here is specific for Erv1/ALR and can be used to reveal normal functions and disease mechanisms in mammalian mitochondria.

RESULTS

A Chemical Screen to Identify Inhibitors of Erv1 Oxidase Activity

We previously developed an assay to test the sulfhydryl oxidase activity of recombinant Erv1 protein based on the oxidation of a nonphysiologic substrate, dithiothreitol (DTT), which produces hydrogen peroxide (H_2O_2) (Dabir et al., 2007). H_2O_2 production was measured using a standard fluorometric assay with Amplex Red and horseradish peroxidase (HRP). The assay was adapted in high throughput format, and a chemical screen was conducted on an integrated robotic system with plate scheduling (Figure S1A available online). Briefly, diversity-oriented commercial libraries of 50,000 drug-like compounds from Chembridge (Lumsden et al., 2007; Webb, 2005), Kwon (Castellano et al., 2007), and Asinex (Lumsden et al., 2007) at 10 μM concentration were screened for inhibition of Erv1 activity. Erv1 (10 μM) was aliquoted into 384-well plates followed by compound addition with robotic pinning into the assay wells. DMSO (1%, vehicle) was included in several plate columns as a carrier control with the pinned compounds. As a negative control, 10 μM catalytically inactive Erv1 (Erv1C133S) was also aliquoted into several plate columns. Incubation of the pinned compounds with Erv1 for 1 hr at 25°C was followed by addition of Amplex Red-HRP and then DTT (20 μM) to initiate the oxidase assay. After 12 min, the reaction was in the kinetic linear range and a high signal-to-noise ratio was achieved. Fluorescence intensity was measured, and reactions that were inhibited by more than 50% were picked as potential Erv1 inhibitors and selected for secondary analysis. In total, 184 primary candidate inhibitors were identified (Figure S1B). Forty plates were processed with a Z′ greater than 0.8 across the screen, indicating that the screen was consistent and robust.

To eliminate false positives, a counter screen was used to test whether the small molecule compounds directly inhibited the Amplex Red-HRP assay. H_2O_2 (800 nM) was reacted with Amplex Red-HRP in the presence of the small molecules; this is the approximate amount of H_2O_2 that was produced by Erv1 during the assay. Those compounds that did not inhibit the Amplex Red assay directly and showed >50% inhibition of Erv1 activity (~29 compounds) were selected for additional characterization and designated as *mito*chondrial protein import *blo*ckers from the *C*arla *K*oehler lab (MitoBloCK) compounds based on their potential to inhibit Erv1 activity. Of these potential "lead" inhibitors, MitoBloCK-6 was chosen for additional analysis. Figure S1C verifies that MitoBloCK-6 does not directly hinder the Amplex Red-HRP reaction.

MitoBloCK-6 Inhibits Erv1 Activity In Vitro

MitoBloCK-6 is 2,4-dichloro-6-((((((phenylamino)phenyl)imino)methyl)phenol) from the Chembridge library (Figure 1A), consisting of a 3,5-dichlorosalicylaldehyde derivative. Upon reordering, MitoBloCK-6 showed the same Erv1 inhibitory activity as the original aliquot from the Chembridge library. The inhibitory concentration at which Erv1 protein activity is reduced by 50% (IC_{50}) for MitoBloCK-6 in the in vitro Amplex Red-HRP assay was 900 nM (Figure 1B). We also tested MitoBloCK-6 as an inhibitor of ALR (Farrell and Thorpe, 2005) and the yeast paralog in the endoplasmic reticulum, Erv2 (Gross et al., 2002), using the in vitro Amplex Red-HRP assay. The IC_{50} for MitoBloCK-6-inhibiting ALR and Erv2 was 700 nM and 1.4 μM, respectively (D.V.D. and C.M.K., unpublished data).

To determine whether MitoBloCK-6 generally impaired redox active enzymes, we investigated the oxidative folding properties of protein disulfide isomerase (PDI). MitoBloCK-6 did not inhibit the ability of PDI to reduce insulin (Figure S1D). Because MitoBloCK-6 may potentially hinder flavin adenine dinucleotide (FAD)-containing enzymes, succinate dehydrogenase activity of the mitochondrial respiratory chain was measured in the presence of MitoBloCK-6 (Figure S1E). Isolated mitochondria were incubated in a Clarke-type oxygen electrode, and oxygen consumption was measured with succinate addition. The oxygen consumption rate was indicative of well-coupled mitochondria, and subsequent addition of DMSO vehicle or MitoBloCK-6 did not alter the oxygen consumption rate. As controls, succinate dehydrogenase activity was disrupted with the inhibitor malonate, and carbonyl cyanide *m*-chlorophenylhydrazone (CCCP) addition indicated that respiring mitochondria could be uncoupled. Because a 3,5-dichlorosalicylaldehyde is a potential degradation product of MitoBloCK-6 and the 3,5-dichlorosalicylaldehyde moiety may instead inhibit Erv1 (Doorn and Petersen, 2003), commercially available 3,5-dichlorosalicylaldehyde replaced MitoBloCK-6 in the in vitro Amplex Red-HRP assay (Figure 1C). The addition of 100 μM 3, 5-dichlorosalicylaldehyde did not inhibit Erv1 activity. We assessed MitoBloCK-6 stability in our screening conditions at pH 6.5 and 7.4 using liquid chromatography-mass spectrometry (LC-MS) analysis (Figure S2A). Analysis at pH 3.4 was also included, because an acidic pH favors hydrolysis of the imine linkage to release the 3,5-dichlorosalicylaldehyde (Kirdant et al., 2011). MitoBloCK-6 was stable over this pH range, as supported by a similar retention time (3.03 min) and a constant area under the curve in the LC-MS analysis (Figure S2A).

Because aldehydes covalently modify lysine residues in proteins by forming a Schiff base (Volkmann et al., 2011; Yamagata et al., 1993), we tested whether a potential aldehyde derived from MitoBloCK-6 covalently modified Erv1 using mass spectrometry (Figure S2B). The addition of 75 μM 3, 5-dichlorosalicylaldehyde to 25 μM Erv1 yielded a spectrum with a single, minor peak at 175 Da, which corresponds to a small amount (<5%) of the 3, 5-dichlorosalicylaldehyde bonding to one position in Erv1; in contrast, most of the Erv1 migrated as the unmodified protein, indicating that the lysine residues in Erv1 are not highly reactive.

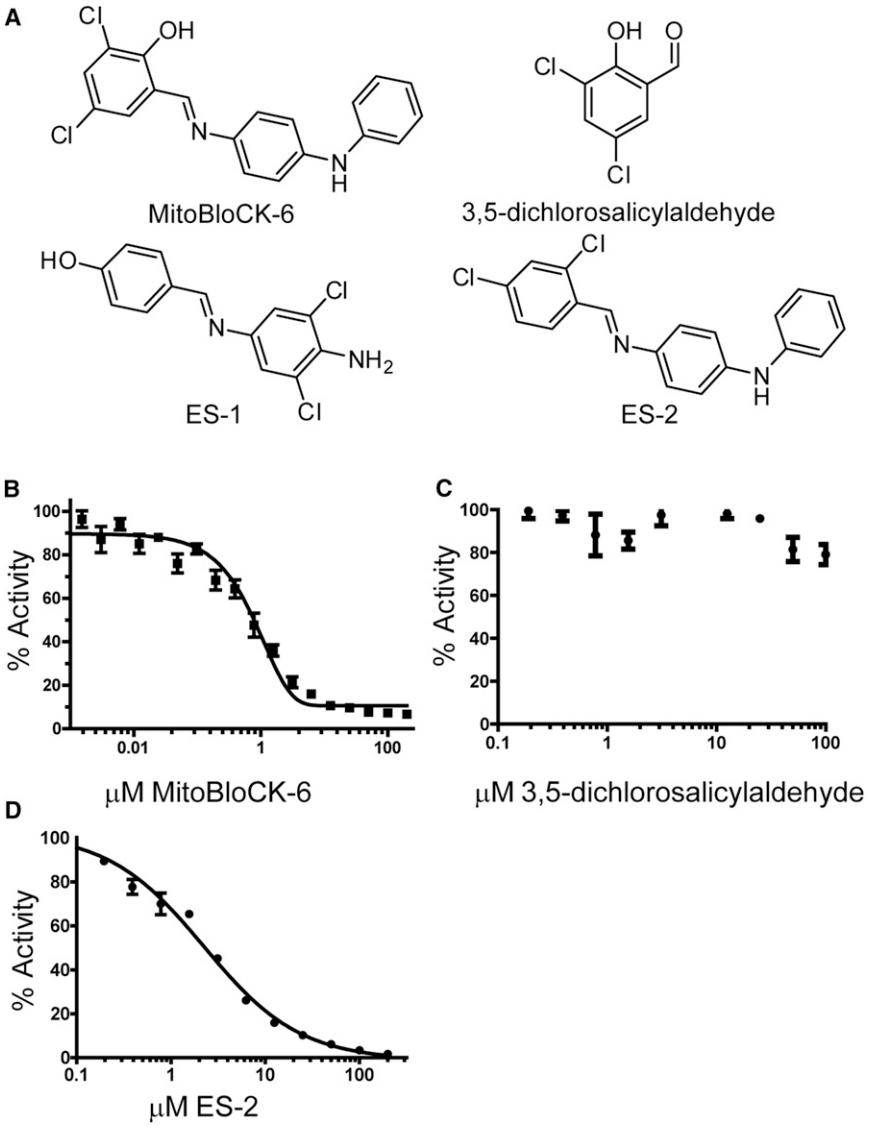

Figure 1. MitoBloCK-6 Inhibits Erv1 Activity

(A) The structure of MitoBloCK-6, Erv1 SAR compound-1 (ES-1) and compound-2 (ES-2), and 3,5-dichlorosalicyclaldehyde.

(B) IC_{50} analysis of MitoBloCK-6 in the in vitro Erv1 activity assay. Ten micromolar Erv1 was incubated with varying concentrations of MitoBloCK-6, as described for the chemical screen.

(C) As in (B), IC_{50} analysis with 3,5-dichlorosalicylaldehyde and Erv1.

(D) As in (B), IC_{50} analysis with ES-2 and Erv1 (average ± SD, n = 3).

See also Figures S1 and S2.

Using lysozyme as a control protein, a small fraction of 3, 5-dichlorosalicylaldehyde again attached covalently, but most of the lysozyme was unmodified (Figure S2C). MitoBloCK-6 (75 μM) addition to Erv1 (25 μM) generated a spectrum in which a small fraction (<3%) of MitoBloCK-6 likely degraded to 3, 5-dichlorosalicylaldehyde that covalently modified Erv1 (Figure S2B); MitoBloCK-6 was specific for Erv1, because the lysozyme spectrum lacked a similar peak that was shifted by 175 Da and additional peaks were not detected (Figure S2C). As a control for the assay, formaldehyde treatment to lysozyme yielded a spectrum in which unmodified lysozyme was replaced with lysozyme bonded with at least 7–9 formaldehyde groups (Figure S2C). Thus, MitoBloCK-6 is a stable compound that does not markedly bond to Erv1.

MitoBloCK-6 Inhibits Erv1-Dependent Import in Mitochondria

The import of Erv1 substrates was tested with an in organello import assay. Substrates included twin CX_9C proteins (Mia40, Cmc1, Cox19, and Cox17), twin CX_3C protein Tim8, and Erv1 (Figures 2 and S3; Hofmann et al., 2005; Horn et al., 2008; Riemer et al., 2011; Terziyska et al., 2007). Energized mitochondria were preincubated with 20–50 μM MitoBloCK-6 or 1% DMSO for 15 min, followed by the addition of the radiolabeled substrate. A time course assay was performed, and aliquots were removed and treated with protease to remove nonimported precursors. Import of the twin CX_9C proteins and Erv1 was strongly decreased, whereas the import of Tim8 was impaired by 40% upon treatment with MitoBloCK-6 compared to import in presence of 1% DMSO. We also investigated the import of additional substrates, Tim23 and ADP/ATP carrier (AAC) of the TIM22 import pathway, and Su9-dihydrofolate reductase (DHFR), cyt b_2-DHFR, and Hsp60 of the TIM23 import pathway (Figures 3 and S3). At 20 μM, the import of Tim23 and AAC was decreased by approximately 50% (Figures 3A and 3B), whereas the import of TIM23 substrates was not impaired, even with 50 μM MitoBloCK-6 (Figures 3C, S3A, and S3B).

Given that Erv1 played a role in the import of TIM22 substrates, we investigated the import of AAC using blue-native (BN) gel analysis (Figure 3D). Previous studies have defined the steps of AAC translocation from the cytosol to the inner membrane using mutants and biochemical manipulations (Curran et al., 2002; Ryan et al., 1999; Truscott et al., 2002). Specifically, AAC accumulates with the TOM machinery in a 500 kDa complex in the *tim10-2* mutant or in the absence of ATP, and then is passed to the Tim9-Tim10 complex; the mature form of AAC subsequently assembles as a dimer in a 90 kDa complex in the inner membrane. After importing AAC in the presence of MitoBloCK-6 or control DMSO, the mitochondria were solubilized in 1% digitonin and separated on BN gels followed by autoradiography. In the presence of DMSO, AAC accumulated in the 90 kDa complex, which is indicative of an assembled AAC dimer (AAC^2). Moreover, the AAC dimer was protected from exogenous protease, verifying that AAC translocated to the inner

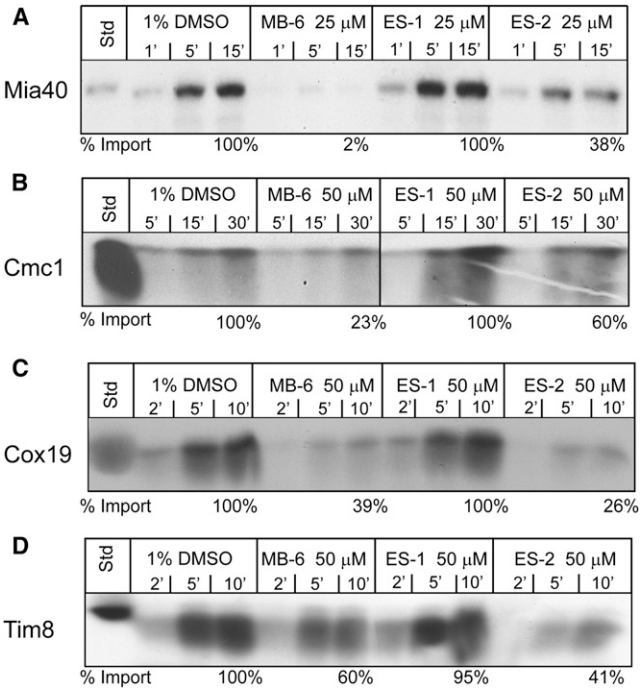

Figure 2. MitoBloCK-6 Inhibits the Import of Substrates of the Mia40/Erv1 Pathway

Radiolabeled precursors were imported into WT mitochondria in the presence of 25 or 50 μM MitoBloCK-6, 50 μM SAR compounds, or the control 1% DMSO. Nonimported precursor was removed by protease treatment. Precursors included (A) Mia40, (B) Cmc1, (C) Cox19, and (D) Tim8. A 10% standard (Std) from the translation reaction is included. Import reactions were quantitated using a BioRad FX Molecular Imager and the affiliated Quantity 1 software; 100% was set as the amount of precursor imported into WT mitochondria at the endpoint in the time course.

See also Figure S3 and Table S1.

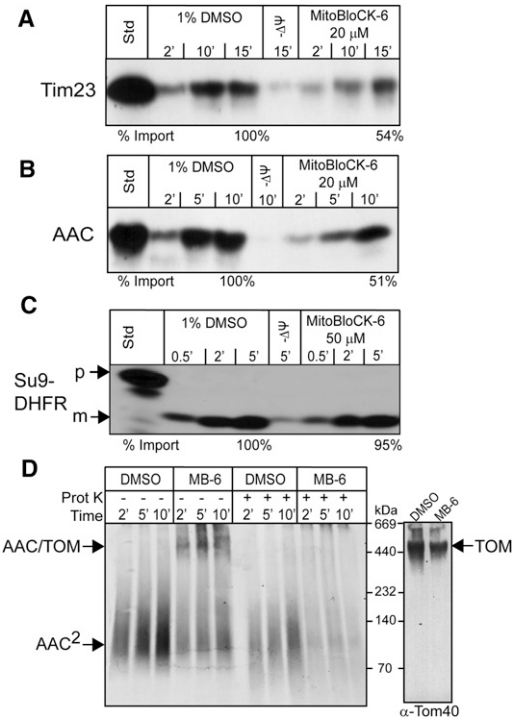

Figure 3. MitoBloCK-6 Inhibits the Import of Substrates of the TIM22 Import Pathway but Not the TIM23 Import Pathway

(A–C) As in Figure 2, import assays were performed. Precursors included TIM22 import substrates (A) Tim23 and (B) AAC and (C) TIM23 substrate Su9-DHFR. Aliquots were removed at the indicated time points, and samples were treated with carbonate extraction to confirm that Tim23 and AAC were inserted into the inner membrane.

(D) AAC was imported in the presence of DMSO or 25 μM MitoBloCK-6, aliquots were removed at indicated time points, and samples were subjected to Blue-Native PAGE analysis followed by autoradiography (left panel) or immunoblotted with antibodies against Tom40 (right panel). AAC^2 marks the AAC dimer, and AAC/TOM marks AAC that accumulates in the TOM complex. Percent import calculated as in Figure 2.

See also Table S1.

membrane. In contrast, the addition of MitoBloCK-6 resulted in AAC accumulation in a 500 kDa complex with the TOM complex (Figure 3D), and this AAC intermediate was sensitive to protease, confirming localization at the outer membrane. Analysis with MitoBloCK-6 supports a role for Erv1 in transferring AAC from the TOM complex to the Tim9-Tim10 complex in the intermembrane space. Therefore, in addition to the cysteine-rich substrates, Erv1 plays a key role in the TIM22 import pathway.

To confirm specificity of MitoBloCK-6, we purchased two additional compounds, termed *E*rv1-structure-activity relationship (SAR) (ES)-1 and ES-2 for an abbreviated SAR study (Figure 1A). ES-2 but not ES-1 (D.V.D. and C.M.K., unpublished data) inhibited Erv1 function in the in vitro assay with an IC_{50} of 2.2 μM (Figure 1D). When included in the import assays, ES-2 mirrored MitoBloCK-6 in its ability to impair import, but ES-1 had no effect (Figures 2, S3C, and S3D). Thus, ES-2 and MitoBloCK-6 seem to specifically inhibit Erv1 function, but ES-1, like 3,5-dichlorosalicylaldehyde, did not abrogate Erv1 function.

To verify that mitochondrial Erv1 is the target of MitoBloCK-6, an increased abundance of Erv1 should require an increased MitoBloCK-6 concentration to inhibit protein import. Previously, we designed a yeast strain, in which Erv1 with a C-terminal hexahistidine tag (designated ↑Erv1) was expressed from a high-copy plasmid (Dabir et al., 2007).This strain contained an approximate 5-fold increase in Erv1 with no aberrant phenotypes detected. The import of Mia40, Cmc1, and AAC proteins was tested in isolated wild-type (WT) and ↑Erv1 mitochondria. For Mia40 and Cmc1, the concentration of MitoBloCK-6 that was required to inhibit import increased from 10 μM to 50 μM (Figures 4A and 4B). A similar trend was detected for AAC import with a concentration increase from 15 μM to 30 μM (Figure 4C). Combined, the data strongly support that Erv1 is the target of MitoBloCK-6.

To evaluate the cell-based activity of MitoBloCK-6, we also determined the *m*inimum *i*nhibitory *c*oncentration required to inhibit the growth of yeast by 50% (MIC_{50}) with the *Δpdr5Δsnq2* yeast strain, in which the genes for the multidrug resistance pumps *PDR5* and *SNQ2* were disrupted in the wild-type strain (Duncan et al., 2007; Hasson et al., 2010). Deletion of these pumps increases the steady state intracellular concentration of

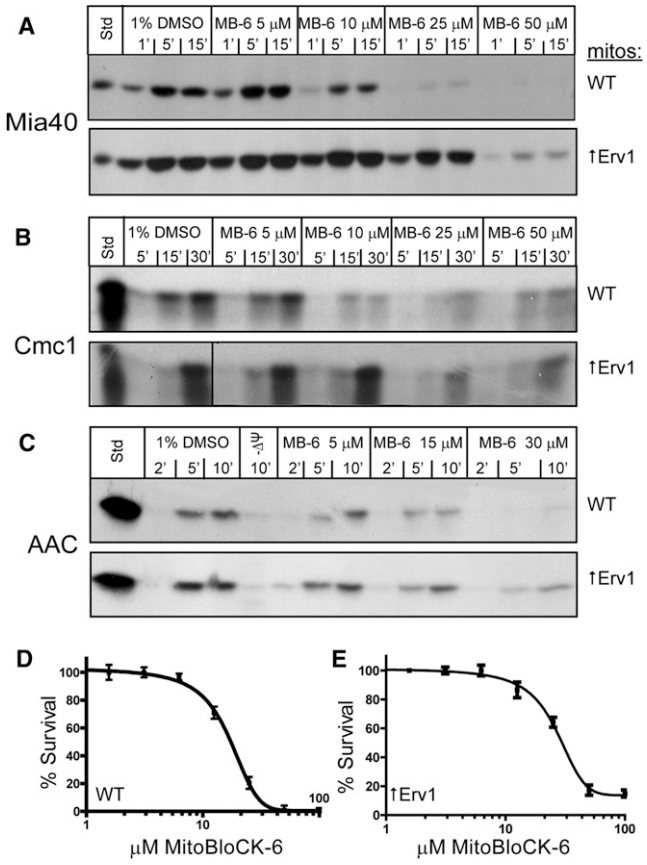

Figure 4. Inhibition of Import by MitoBloCK-6 Is Dependent on the Concentration of Erv1 in Mitochondria

(A–C) Import assays of precursors (A) Mia40, (B) Cmc1, and (C) AAC were performed as described in Figure 2 into mitochondria derived from wild-type (WT) yeast or yeast overexpressing Erv1 with a hexahistidine tag (↑Erv1) (Dabir et al., 2007). The concentration of MitoBloCK-6 was varied from 5 to 50 μM as indicated. A 10% standard (Std) from the translation reaction was included.

(D) MIC_{50} analysis of the WT yeast strain lacking the drug pumps (Δ*pdr5* Δ*snq2*) with varying concentrations of MitoBloCK-6 (average ± SD, n = 6).

(E) As in (D), MIC_{50} analysis of the Δ*pdr5* Δ*snq2* yeast strain that overexpresses Erv1-His from a high-copy plasmid (↑Erv1) (average ± SD, n = 6).

See also Figure S4 and Table S1.

drugs in yeast. The MIC_{50} was 15.2 μM (Figure 4D), which is similar to the IC_{50} concentration that inhibited protein import. As in the import assays (Figures 4A–4C), we measured the MIC_{50} with the *Δpdr5Δsnq2* strain overexpressing Erv1 from a high-copy plasmid (Dabir et al., 2007). The MIC_{50} increased to 28.3 μM when Erv1 was overexpressed (Figure 4E).

Mitochondria Are Not Damaged by MitoBloCK-6

A potential mechanism by which MitoBloCK-6 could alter protein translocation is to nonspecifically permeabilize membranes, resulting in the release of mitochondrial proteins, particularly from the IMS. We have previously shown that MitoBloCK-2, an inhibitor of the TIM22 import pathway, nonspecifically permeabilizes mitochondrial membranes (Hasson et al., 2010). We incubated energized mitochondria with 1% DMSO or MitoBloCK-6 followed by centrifugation. Released proteins were recovered in the supernatant fraction and analyzed by Coomassie staining for the collective release of proteins (Figure S4A) and by immunoblot assay for key proteins (Figure S4B). The results from Coomassie staining indicated that MitoBlock-6 did not alter mitochondrial membrane integrity, because proteins were not released into the supernatant fraction (Figure S4A). Similarly, immunoblot analysis showed that marker proteins aconitase (matrix), AAC and Tim54 (inner membrane), and IMS proteins Mia40, Ccp1, and cyt *c* were not released with MitoBloCK-6 or DMSO treatment (Figure S4B).

Another potential mechanism by which MitoBloCK-6 may disrupt protein translocation is indirect, by dissipation of the membrane potential ($\Delta\psi$) or disruption of oxidative phosphorylation, both of which can be measured with a Clark-type oxygen-sensing electrode (Figure S4C; Claypool et al., 2008). Isolated mitochondria were incubated in a 0.5 ml chamber at 25°C with an oxygen electrode, and respiration was initiated with reduced nicotinamide adenine dinucleotide. The measured oxygen consumption rate was indicative of well-coupled mitochondria. The subsequent addition of DMSO vehicle or MitoBloCK-6 did not alter the oxygen consumption rate. As a control, mitochondria were treated with the protonophore CCCP, and respiration increased drastically, indicative of uncoupled mitochondria (Figure S4C). Taken together, MitoBloCK-6 does not alter mitochondrial function or disrupt mitochondrial integrity and functions biochemically as a specific inhibitor of Erv1.

MitoBloCK-6 Impairs Substrate Oxidation

To determine how MitoBloCK-6 inhibited Erv1 function, we investigated whether MitoBloCK-6 altered Erv1 interactions with partner proteins in isolated mitochondria (Figure 5A). MitoBloCK-6 was preincubated with mitochondria isolated from the Erv1-His strain followed by solubilization in 1.0% digitonin, and Erv1-His was purified with Ni^{+2} agarose. In DMSO-treated cells, a small fraction of the Mia40 and cyt *c* copurified with Erv1, as reported previously (Tienson et al., 2009). However, in the presence of MitoBloCK-6, binding of Mia40 and cyt *c* to Erv1 was decreased by 75% and 95%, respectively (Figure 5A).

If MitoBloCK-6 interferes with Mia40-Erv1 binding, then the oxidation of substrates may be inhibited in vitro. We therefore evaluated Tim13 oxidation and subsequent production of H_2O_2 in vitro (Figure 5B; Tienson et al., 2009). Erv1 was preincubated with DMSO or MitoBloCK-6 for 1 hr at 25°C. Then, the oxidation of Tim13 was reconstituted by incubating reduced Tim13 with catalytic amounts of Erv1 and Mia40 in an aerobic environment. Oxidation was monitored over a time course by the addition of 4-acetamido-4-maleimidylstilbene-2, 2-disulfonic acid (AMS) followed by nonreducing SDS-PAGE and immunoblot analysis with antibodies against Tim13. AMS addition causes an increase in molecular mass of 0.5 kDa per addition to a cysteine residue. In the presence of DMSO, reconstitution proceeded normally and approximately 80% was oxidized after 3 hr. By contrast, only 15% of Tim13 was oxidized in the presence of MitoBloCK-6 (Figure 5B). As Tim13 was oxidized, H_2O_2 production was monitored using the Amplex Red-HRP assay (Figure 5C; Tienson et al., 2009). The addition of MitoBloCK-6 caused a significant decrease in H_2O_2 production compared to the control reactions. We also tested the oxidation of Cmc1 (Bourens et al., 2012), a substrate of Mia40/Erv1 pathway, with Erv1

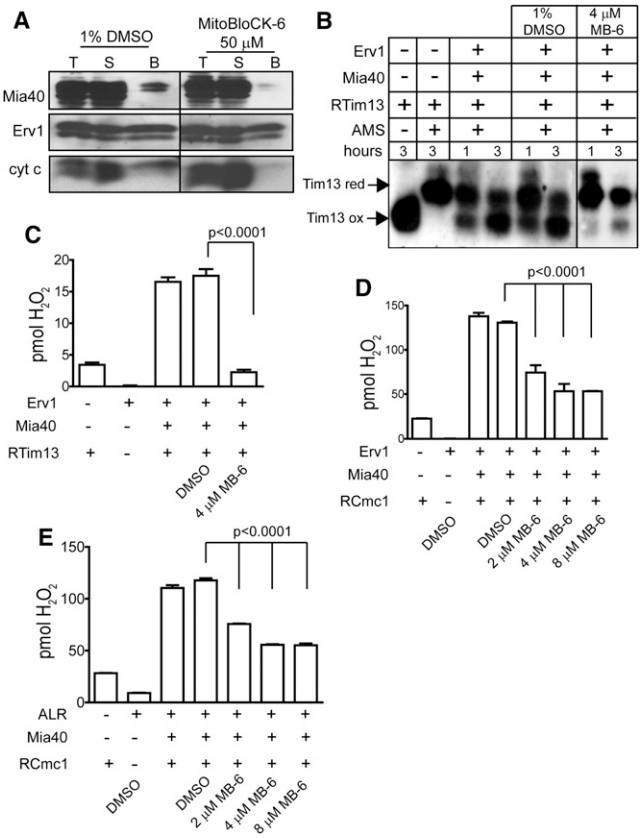

Figure 5. MitoBloCK-6 Impairs Substrate Oxidation In Vitro and Disrupts Erv1 Binding

(A) Mitochondria from a strain expressing C-terminal histidine-tagged Erv1 were incubated with 50 μM MitoBloCK-6 or 1% DMSO for 30 min at 25°C followed by solubilization in 1% digitonin buffer. As a control, 100 μg of extract was withdrawn (T), and 500 μg lysate was incubated with Ni^{+2}-agarose beads. The beads were washed and bound proteins (B) were eluted with SDS-PAGE sample buffer. To test effectiveness of binding, 100 μg of the unbound protein fraction (S) was also included. Proteins were analyzed by immunoblotting with polyclonal antibodies against Mia40, Erv1, and cyt *c*.

(B) Recombinant Erv1 was preincubated with MitoBloCK-6 or 1% DMSO for 1 hr at 25°C, and then Erv1 (1 μM) was incubated with reduced Tim13 (15 μM) and Mia40 (1 μM) in a time-course assay (Tienson et al., 2009). Aliquots were removed at the indicated times, and free thiols on Tim13 were modified with AMS addition. Oxidized and reduced Tim13 were detected by nonreducing SDS-PAGE and immunoblotting with antibodies against Tim13.

(C–E) The same reconstitution assay was performed as in (B) with reduced Tim13 (C), reduced Cmc1 (D and E) or mammalian ALR (E), and H_2O_2 production was monitored over a 30 min time period with the indicator Amplex Red and displayed as pmol H_2O_2 (one-way ANOVA, n = 3).

(Figure 5D) and ALR (Figure 5E). An increase in MitoBloCK-6 concentration correlated with a dose-dependent decrease in H_2O_2 production. Thus, MitoBloCK-6 specifically blocks the oxidation of Tim13 and Cmc1 in vitro for both Erv1 and ALR.

As an additional test for MitoBloCK-6 inhibition of Erv1 oxidase activity, we measured the oxygen consumption rate by Erv1 with an oxygen electrode in the presence of excess DTT (Dabir et al., 2007). When Erv1 was added alone or with DMSO, the oxygen consumption rate was similar (Figure S4D). By contrast, the addition of MitoBloCK-6 resulted in a concentration-dependent decrease in the oxygen consumption rate. Results from these analyses show that MitoBloCK-6 selectively inhibits Erv1 and ALR oxidase activity in vitro.

MitoBloCK-6 Inhibits ALR Function in Vertebrate Mitochondria

The long-term goal in developing the MitoBloCK compounds is to adapt them for studies in vertebrate mitochondria, such as recapitulating biochemical phenotypes similar to those in cells derived from patients with mutations in ALR (Di Fonzo et al., 2009). In addition, MitoBloCK-6 may be useful for studies of apoptosis, iron sulfur cluster and heme export (Dabir et al., 2007), and cell differentiation (Todd et al., 2010b), because ALR has been implicated in these pathways. Since MitoBloCK-6 inhibits ALR oxidase activity in vitro, we asked whether MitoBloCK-6 disrupts mitochondrial function in mammalian cells by investigating mitochondrial morphology, a general readout for mitochondrial defects. HeLa cells were transiently transfected with mitochondrial matrix-targeted Su9-EGFP and colabeled with Mitotracker-Red (Figure S5A). Cells were treated with 50 μM MitoBloCK-6 for 12–16 hr, and mitochondrial morphology and integrity was visualized by microscopy. In cells treated with DMSO, Su9-EGFP colocalized with Mitotracker staining and the mitochondrial network was distributed as in the untreated cells. However, the addition of CCCP caused the mitochondrial network to collapse around the nucleus. MitoBloCK-6 addition did not disrupt the mitochondrial network (Figure S5A), even at concentrations up to 100 μM MitoBloCK-6 (unpublished data). We also examined cell viability with a 1-(4, 5-dimethylthiazol)-3, 5-diphenylformazan (MTT) assay (Figure S5B). MitoBloCK-6 (100 μM) did not significantly reduce cell viability. In addition, treatment of HEK293 cells with MitoBloCK-6 showed similar results (D.V.D. and C.M.K., unpublished data). Because Erv1 passes electrons to cyt *c*, ALR may play a role in apoptosis in mammalian cells. Therefore, we queried specifically whether cyt *c* was released in cells exposed to MitoBloCK-6 (Figure S5C). Cells incubated with a positive control, staurosporine, showed cyt *c* release and detection in the cytoplasmic fraction as an indication of apoptosis. However, 50 μM MitoBloCK-6 treatment for 12–16 hr failed to initiate cyt *c* release (Figure S5C). Whereas MitoBloCK-6 inhibits ALR function in vitro, this inhibitory activity is surprisingly lacking in HeLa and HEK293 cells.

ALR was identified in a set of common genes that are enriched in embryonic, neuronal, and hematopoietic stem cells (Ivanova et al., 2002; Ramalho-Santos et al., 2002), and ALR has a prosurvival role in maintaining human embryonic stem cells (hESCs) (Todd et al., 2010a). Thus, ALR may have a specific and different role in hESCs and induced pluripotent stem cells than in differentiated cells, such as HeLa and HEK293 cells. Therefore, we determined whether MitoBloCK-6 affected hESC survival. HSF1 hESCs and normal human dermal fibroblasts, which represent a differentiated cell type, were exposed with 20 μM MitoBloCK-6 or 0.1% DMSO and visualized using bright field microscopy (Figure S6A), including staining with Coomassie brilliant blue to visualize colony morphologies (Figure S6B; Mochizuki and Furukawa, 1987). MitoBloCK-6 exposure resulted in marked HSF1 cell death, whereas DMSO exposure did not cause cell death or alter overall colony morphology. MitoBlock-6 may trigger stem cell apoptosis. Release of cyt *c* was examined in

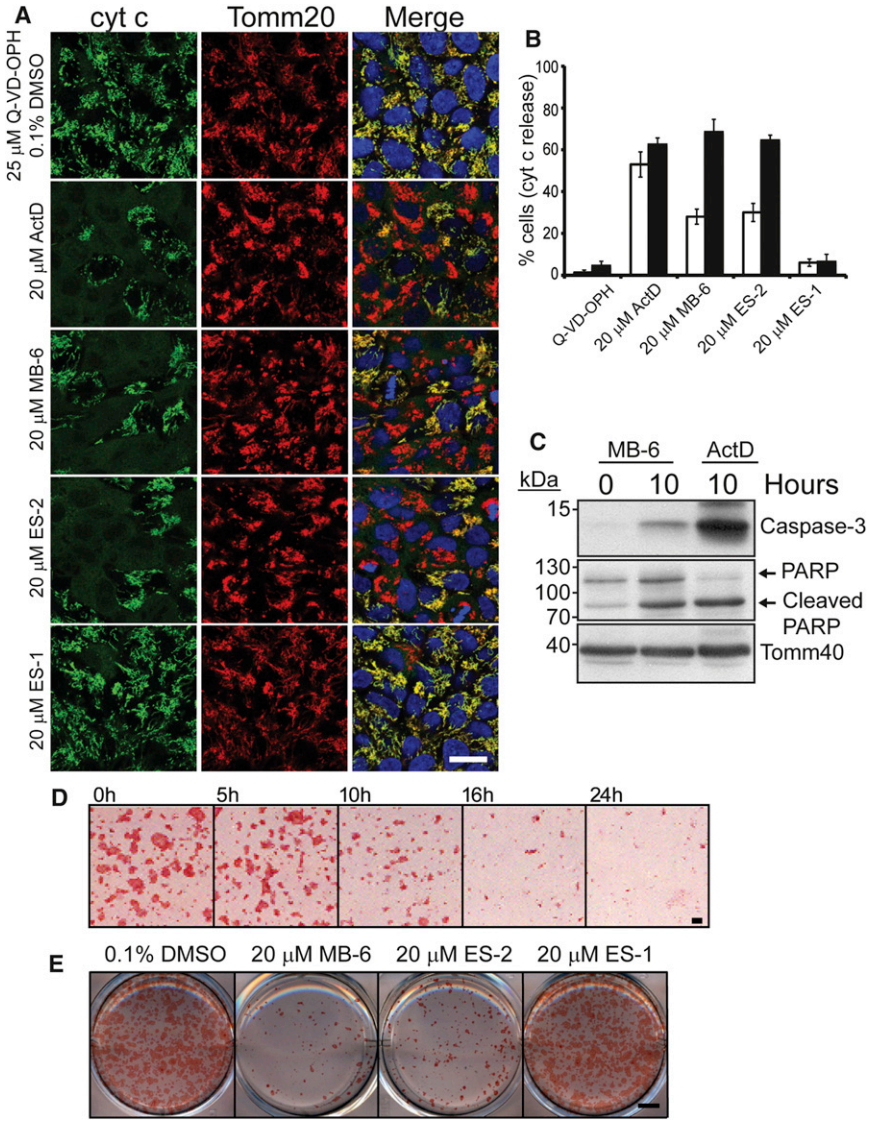

Figure 6. MitoBloCK-6 Induces Apoptosis in hESCs

(A) HSF1 cells were treated with 20 μM MitoBloCK-6, ES-1, or ES-2 for 8 hr. As a positive control, apoptosis was induced in cells by treatment with 20 μM actinomycin D (ActD) for 8 hr. Downstream caspases were inhibited by simultaneous addition of 25 μM Q-VD-OPH (caspase inhibitor) for 8 hr. Cells were fixed and analyzed by immunofluorescence microscopy using antibodies against cyt *c* (green) and Tomm20 (red). Merged images are also depicted in panels with Hoescht staining (blue) to mark nuclei. Scale bar, 20 μm.

(B) Quantification of data obtained in (A) and represented as percentage of cells that lost the mitochondrial cyt *c* staining at 5 hr (white bars) or 8 hr (solid black bars) but retained Tomm20 staining. Data were collected from three independent experiments. Error bars represent standard deviation (average percent ± SD; n = 4).

(C) As in (A), HSF1 cells were treated with 20 μM MitoBloCK-6 or 20 μM ActD for the indicated time. Whole cell extracts were analyzed by SDS-PAGE and immunoblotted with antibodies for caspase-3 fragment and PARP. Tomm40 was included as a loading control.

(D) As in (A), HSF1 cells were treated with 20 μM MitoBloCK-6 for the indicated times, followed by staining for alkaline phosphatase activity. Scale bar, 500 μm.

(E) Analysis of alkaline phosphatase activity in HSF1 cells after treatment with 0.1% DMSO, 20 μM MitoBloCK-6, 20 μM ES-1, or 20 μM ES-2 for 16 hr. Scale bar, 500 μm.

See also Figures S5 and S6.

HSF1 cells exposed to MitoBloCK-6 (Figure 6A) using antibodies against cyt *c* and visualized by fluorescence microscopy (Waterhouse et al., 2001). MitoBloCK-6 addition resulted in a shift in cyt *c* localization from mitochondria (marked with Tomm20) into the cytosol (shown as diffuse staining that did not overlap with Tomm20 staining). SAR compound ES-2, but not ES-1, also caused cyt *c* release from mitochondria. Quantification indicated that the number of cells in which cyt *c* was released was similar with addition of MitoBloCK-6, ES-2, or actinomycin D, a known apoptosis inducer (Figure 6B). In contrast, treatment with the broad caspase inhibitor N-(2-Quinolyl)valyl-aspartyl-(2,6-difluorophenoxy)methyl ketone (Q-VD-OPH) and the vehicle 0.1% DMSO did not alter mitochondrial morphology or cause cyt *c* release. In addition, downstream events in apoptosis, poly-ADP-ribose polymerase (PARP) and caspase-3 cleavage, were also detected with MitoBloCK-6 exposure (Figure 6C).

To support that MitoBloCK-6 specifically inhibited the survival of hESCs and not of differentiated cells, HSF1 cells were induced to differentiate with 10 μM retinoic acid followed by MitoBloCK-6 exposure (Figure S6). Again, the images show that colony morphology remained intact when HSF1 cells were differentiated with retinoic acid treatment and cells did not die. To assess the earliest time point at which MitoBloCK-6 perturbed hESC viability, a time course assay was performed and hESCs were stained for alkaline phosphatase activity (Shamblott et al., 1998). hESC viability started to decline after 5 hr posttreatment (Figure 6D). Twenty micromolar SAR compounds ES-1 and ES-2 were applied to hESCs and stained for alkaline phosphatase activity. Whereas ES-1 had no effect on cell growth, ES-2 inhibited cell growth similar to MitoBloCK-6 (Figure 6E). Taken together, MitoBloCK-6 does not inhibit mitochondrial function in differentiated cells, but hESCs were susceptible to MitoBloCK-6 and apoptosis was induced. The data suggest a key role for ALR in hESC maintenance and show that MitoBloCK-6 is a small molecule reagent that identifies this function.

Having characterized the effects of MitoBloCK-6 in vitro and in primary cell culture systems, we applied MitoBloCK-6 to developing zebrafish embryos, which is a useful in vivo vertebrate model. The effect of MitoBlock-6 on mitochondrial function and zebrafish development was tested using previously established parameters (Mendelsohn et al., 2006; Murphey

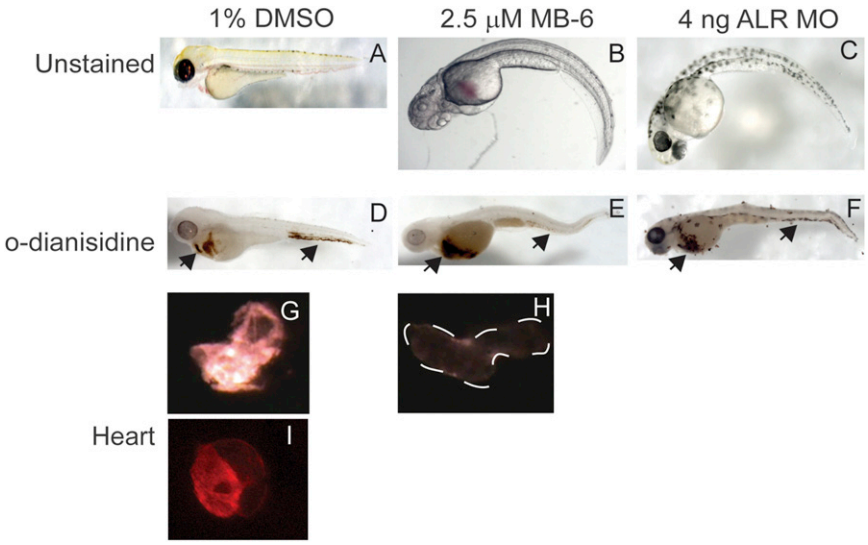

Figure 7. MitoBloCK-6 Treatment Impairs Cardiac Development in Zebrafish

Embryos (3 hpf) were treated with 2.5 μM MitoBloCK-6 (B, E, and H) or 1% DMSO (A, D, and G) or embryos were injected with an ATG morpholino against ALR (C and F). Development was visualized by microscopy at 72 hpf (A–C). Erythrocytes were visualized by o-dianisidine staining at 72 hpf (D–F); arrows indicate regions of red blood cell accumulation in wild-type fish. Fluorescence microscopy of zebrafish hearts (72 hpf) that contained a mitochondrial-targeted DsRed included embryos treated with 1% DMSO (G), 2.5 μM MitoBloCK-6 (H), and buffer only (I).
See also Figure S7.

and Zon, 2006). Zebrafish embryos were placed in either 1% DMSO or 2.5 μM MitoBloCK-6 at 3 hr postfertilization (hpf) and allowed to develop until 72 hpf. Higher concentrations of MitoBloCK-6 were toxic to the fish. MitoBloCK-6- but not DMSO-incubated embryos displayed ventral curvature of the body and cardiac edema (Figures 7A and 7B). Furthermore, we also treated fish with MitoBloCK-6 from 3–24 hpf, followed by removal of MitoBloCK-6, and the zebrafish embryos were identical to those exposed to DMSO at 72 hpf, indicating that the effects of MitoBloCK-6 are reversible (M.E.J. and C.M.K., unpublished data). Because ALR may play a role in FeS cluster assembly and export (Lange et al., 2001), erythropoiesis may be defective (Shaw et al., 2006). Therefore, embryos were stained with o-dianisidine, which binds to heme (Lumsden et al., 2007), as a method to visualize hematopoietic development. Whereas embryos exposed to 1% DMSO or MitoBloCK-6 showed normal hematopoiesis, embryos treated with MitoBloCK-6 showed erythrocyte pooling along the yolk sac prior to entering the lower chamber of the heart and an absence of red blood cells in the tail (Figures 7D and 7E). To assess if the observed phenotypes were caused by ALR inhibition via MitoBloCK-6, one-cell embryos were also injected with 4 ng of a translation initiation codon (ATG) morpholino targeted to ALR (Figures 7C and 7F). This morpholino prevents ALR translation in embryos. The phenotypes observed from the morpholino-injected embryos were identical to that of MitoBlock-6 exposure, suggesting that ALR is targeted. Cardiac development was also investigated in a transgenic zebrafish line, in which DsRed is targeted to mitochondria under control of the heart-specific cardiac myosin light chain promoter *cmlc2* (Figures 7G–7I; Shu et al., 2007). Cardiac development at day 3 in embryos exposed to DMSO was similar to that of wild-type fish in that the heart is looped and the mitochondria are also very bright (Figures 7G–7I). In contrast, MitoBloCK-6 exposure retarded cardiac development in that the hearts failed to loop by day 2, instead becoming stringy and extended. In addition, the mitochondria were less fluorescent (Figure 7H), which is likely indicative of dysfunctional mitochondria. This developmental defect is supported by a decreased heart rate of 50% and 25% in embryos treated with MitoBloCK-6 and the ALR morpholino, respectively.

To confirm that the target of MitoBloCK-6 in vivo is indeed ALR, embryos were treated with suboptimal concentrations of MitoBloCK-6 (1 or 2 μM) and the ATG morpholino (1 or 2 ng) in different combinations (Figure S7). Lower concentrations of either MitoBloCK-6 or ATG morpholino did not impair development; cardiac tissue was relatively normal and Ds-Red fluorescence marking mitochondria was similar to the fish treated with 1% DMSO. As zebrafish were treated with 2 μM MitoBloCK-6 and 1 to 2 ng of ATG morpholino, defects in development were additive. Specifically, the embryos displayed cardiac edema and decreased fluorescence in cardiac tissue; this phenotype was similar to that in embryos treated with either 2.5 μM MitoBloCK-6 or 4 ng ATG morpholino (Figure 7). Taken together, the data strongly suggest that MitoBloCK-6 specifically targets and blocks ALR function in zebrafish, which is marked by impaired cardiac development.

DISCUSSION

We identify MitoBloCK-6 as a selective inhibitor of the Mia40/Erv1 redox-mediated import pathway. Based on the assay in which oxidation of substrate DTT by Erv1 was inhibited, the mechanism by which MitoBloCK-6 may attenuate Erv1 activity is to potentially interfere with binding or electron transfer between Mia40, cyt *c*, and/or oxygen. MitoBloCK-6 is a stable compound. The hydroxyl group at the ortho position likely stabilizes the compound (Crugeiras et al., 2009), and a similar class of molecules has been identified in a small molecule screen for inhibitors of Type III secretion (Nordfelth et al., 2005).

Import of CX_9C proteins was reduced more than CX_3C protein Tim8. Pfanner and colleagues have shown that a ternary complex is formed by the substrate, Mia40, and Erv1 (Stojanovski et al., 2008); MitoBloCK-6 may potentially interfere with the formation of this ternary complex in a substrate-specific manner. Strong inhibition of Mia40 import by MitoBloCK-6 was also unexpected, because full-length Mia40 in yeast uses the TIM23 pathway (as in Figure 2A), but a truncated version, similar to human Mia40, that contains the core cysteine residues uses

the Mia40/Erv1 pathway (Chacinska et al., 2008). That MitoBloCK-6 blocks Mia40 import suggests that the Erv1 pathway may be important for coordinating disulfide assembly in the imported Mia40, because *mia40* mutants with cysteine mutations that prevent correct disulfide bond formation are not viable (Terziyska et al., 2009). Surprisingly, import of substrates of the TIM22 pathway (AAC and Tim23) was also reduced, which suggests a broader role for the Mia40/Erv1 pathway in protein translocation. The potential role of Erv1 in the TIM22 pathway may be difficult to dissect with yeast mutants; a subset of yeast mutants did not show a defect in the carrier import pathway (Mesecke et al., 2005; Rissler et al., 2005), whereas our import studies with *erv1* mutants resulted in general pleiotropic defects in import (D.V.D. and C.M.K., unpublished data). Redox regulation seems to be important in the TIM22 pathway, because the small Tim proteins may undergo redox regulation and the cysteine-rich protein Hot13 may also participate (Curran et al., 2004). Alternatively, MitoBloCK-6 inhibition of Erv1 may change the redox potential of the IMS, which may alter import ability of the small Tim proteins. Additional experiments will be required to determine how MitoBloCK-6 specifically alters the TIM22 pathway.

ALR Has a Key Function in hESC Maintenance and Zebrafish Development

Our strategy of screening with the yeast protein Erv1 was also constructive, because MitoBloCK-6 inhibited the human homolog ALR with an improved IC_{50} of 700 nM. High-resolution crystallography and nuclear magnetic resonance studies of four Erv1 family proteins, *Arabidopsis thaliana* Erv1 (Vitu et al., 2006), rat ALR (Wu et al., 2003), human ALR (Banci et al., 2011), and yeast Erv2 (Gross et al., 2002), reveal that the structure is highly conserved. Thus, our screen has produced small molecules that work across species. This also has been shown in an in vivo screen, in which we determined that MitoBloCK-1 of yeast Tim10 also inhibited Tim10 in mammalian mitochondria (Hasson et al., 2010). Furthermore, Nunnari and colleagues identified mdivi-1 as an inhibitor of the yeast fission component Drp1 (Cassidy-Stone et al., 2008). mdivi-1 also abrogates mammalian Drp1 and retards apoptosis by preventing mitochondrial outer membrane permeabilization.

Whereas MitoBloCK-6 inhibits activity of the Erv1 family in vitro, a surprising finding was that MitoBloCK-6 did not inhibit growth or function of differentiated cells in vivo. An initial reason may be that a factor in the media inhibited MitoBloCK-6 action. However, several types of media were tested, including the permissive hESC media with differentiated cells, and MitoBloCK-6 remained inactive. In contrast, MitoBloCK-6 specifically induced apoptosis in hESCs, suggesting ALR may have a distinct role in pluripotent stem cell maintenance. Published studies support a role for ALR in stem cells, because ALR expression is enriched in embryonic, neuronal, and hematopoietic stem cells (Ivanova et al., 2002; Ramalho-Santos et al., 2002). ALR has been reported to have a prosurvival role in maintaining mouse pluripotent embryonic stem cells by interacting with Drp1 (Todd et al., 2010a). However, Drp1 is a cytosolic protein mediating mitochondrial fission, and it is not apparent how IMS-localized ALR associates with Drp1; our data support the model that ALR inactivation by MitoBlock-6 results in cyt *c* release, and the mitochondrial network collapses as a consequence of apoptosis (Parone et al., 2006). We and others have shown that Erv1 and ALR shuttle electrons to cyt *c* (Bihlmaier et al., 2007; Dabir et al., 2007; Farrell and Thorpe, 2005). In differentiated cells, approximately 85% of the cyt *c* population is distributed in the cristae in association with the respiratory complexes, and 15% is located in the IMS in the region between the inner and outer membrane (Bernardi and Azzone, 1981); this 85% population of cyt *c* is released from the cristae during apoptosis in differentiated cells (Scorrano et al., 2002). However, hESC mitochondria lack numerous cristae and display decreased respiration compared to differentiated cells (Zhang et al., 2011), so the population of cyt *c* that associates with ALR may be the critical pool that is released during apoptosis. As a result of our preliminary finding, MitoBloCK-6 is an excellent tool to understand the contribution of mitochondrial to pluripotent stem cell function and differentiation. In addition, MitoBloCK-6 may be important in translational strategies to remove pluripotent hESCs that "fail-to-differentiate" in hESC transplantation studies. Removal of hESCs prior to transplantation in patients is important because hESCs induce teratomas in the wrong environment (Tang et al., 2011). Additional studies are ongoing to understand how MitoBloCK-6 induces apoptosis in hESCs.

In contrast to differentiated culture cells, zebrafish provide a powerful model system for characterizing ALR function, because cells are not transformed and are in their normal physiologic setting of cell-cell and cell-extracellular matrix interactions (Murphey and Zon, 2006). The embryos are also in simple buffered water, so MitoBloCK-6 uptake may be enhanced. Defects in mitochondrial biogenesis in zebrafish display varied phenotypes. Mutations in the Tomm22 import component result in defects in liver development (Curado et al., 2010), and mutations in Fe-S cluster biogenesis typically impact erythropoiesis (Shaw et al., 2006; Wingert et al., 2005). Indeed, MitoBloCK-6 also elicited gross morphologic and cardiac defects in zebrafish that were akin to ALR downregulation. Overall, characterization of MitoBloCK-6 supports that the chemical approach is valid for developing probes to study protein translocation and understand the role of protein import in development.

EXPERIMENTAL PROCEDURES

High-Throughput Screen for Erv1 Modulators

The primary chemical screen used fresh recombinant Erv1 (in buffer 30 mM 4-(2-hydroxyethyl)-1-piperazineethanesulfonic acid, pH 7.4, 100 mM NaCl, 1 mM EDTA) at a concentration of 10 μM, which was expressed as described previously. A Titertek multidrop (Beckman Coulter) was used to dispense 25 μl Erv1 or 25 μl of catalytically inactive enzyme Erv1C133S into wells of a clear bottom 384-well plate (Greiner Bio One). A Biomek FX (Beckman Coulter) was used to pin transfer 0.5 μl of compound from 1 mM stock or DMSO to respective wells. Approximate screening concentration was 12.5 μM. After completed compound transfer, all plates were incubated at 25°C in a humidified incubator for 1 hr. A Titertek multidrop was used to dispense 15 μl of Amplex Red-HRP (Sigma) mix into all wells of the 384-well plate. The final concentration of Amplex Red and HRP were 46 μM and 0.092 U/ml, respectively. The Amplex Red-HRP solution was shielded from light during the entire experiment. The plates were incubated for an additional 10 min, and then 15 μl of the substrate DTT (20 μM) was added to initiate the reduction of O_2 to H_2O_2. The plates were incubated for 12 min to achieve a maximal signal-to-noise ratio in the kinetic liner range. Plates were then read at an endpoint using an excitation wavelength of 545 nm and an emission wavelength of 590 nm. All operations were performed by an automated plate scheduler to

ensure consistency across the screening run. We chose compounds that inhibited Erv1 activity by greater than 50%. Using a similar screening methodology as above, hit compounds were reconfirmed. Compounds that were available were ordered from Asinex and Chembridge and assayed for IC_{50} using a similar automated technique in 384-well plates, as previously described. Serial dilutions of purchased compounds were performed with robotic automation in 100% DMSO. Subsequently, compounds were pinned into assay plate wells containing 10 μM Erv1, Erv2, or ALR.

Assays in hESCs

The hESC line HSF1 (NIH-UC01; UCLA Embryonic Stem Cell Research Oversight committee-approved) was cultured in Stem Pro SFM (GIBCO) supplemented with 10 ng/ml basic fibroblast growth factor on Matrigel (BD Biosciences)-coated plates under 5% CO_2, 95% air. Differentiation involved culturing cells in Stem Pro SFM with 10 μM retinoic acid (Acros Organics) for 4 days. Cells were treated with the indicated concentration of the MitoBloCK compounds or 0.1% DMSO as a control. For cytochrome *c* release analysis using microscopy, cells were exposed to 20 μM actinomycin D (Sigma), MB-6, ES-1, or ES-2 with 25 μM broad caspase inhibitor Q-VD-OPH (EMD Millipore) (Caserta et al., 2003). Treatment with Q-VD-OPH and 0.1% DMSO alone or in combination did not affect cell morphology. Following treatment, cells were fixed with 3.7% formaldehyde for indirect immunofluorescence study or lysed with Triton buffer (25 mM Tris-HCl pH 7.5, 150 mM NaCl, 1% Triton X-100, 1mM EDTA) for analysis by SDS-PAGE. Bright field images were acquired with Exi Blue (QImaging). Immunofluorescent images were acquired with a 63X oil immersion objective on an LSM 5 PASCAL laser scanning microscope (Carl Zeiss). Antibodies against cyt *c* (BD PharMingen), Tomm20 (Santa Cruz), cleaved caspase-3 (Cell Signaling), and poly-ADP-ribose polymerase (Cell Signaling) were purchased from the indicated vendors. Nuclei were visualized by Hoechst (0.12 μg/ml) staining after straining. Alkaline phosphatase activity staining was performed with the leukocyte alkaline phosphatase kit (Sigma) as per manufacturer's protocol. Coomassie brilliant blue staining was performed by staining cells with Coomassie brilliant blue solution (0.25% Coomassie brilliant blue R250, 45% methanol, 10% acetic acid) for 1 hr at room temperature. Cells were washed with phosphate-buffered saline followed by visualization, as described above.

Statistical Analysis

Quantitative analysis was performed in GraphPad Prism 5 software unless otherwise stated. Statistical tests for significant deviation between samples were performed using one-way ANOVA followed by Bonferroni's posttest. The alpha threshold for significance was <0.05 for all tests.

Assays

MitoBloCK-6 was analyzed using a battery of established in vitro, yeast, mammalian cell-based, and zebrafish assays. These are described in detail in the Supplemental Information. Yeast strains are listed in Table S1.

SUPPLEMENTAL INFORMATION

Supplemental Information includes seven figures, one table, and Supplemental Experimental Procedures and can be found with this article online at http://dx.doi.org/10.1016/j.devcel.2013.03.006.

ACKNOWLEDGMENTS

We thank Dr. A. Barrientos (University of Miami) for the Cmc1 antibody, J. Wijaya, J. Steffen, T. Hioe, S. Irving, and J. Hotter for excellent technical assistance, and Dr. M. Jung (UCLA) for discussions about small molecule chemistry. We acknowledge the use of the Chemical Database Service at Daresbury. This work is supported by CIRM grants RS1-00313 and RB1-01397 (to M.A.T. and C.M.K.) and NIH grants GM073981 (to C.M.K. and M.A.T.), GM61721 (to C.M.K.), MH085683 (to C.M.K.), PNEY018228 (to M.A.T.), P01GM081621 (to M.A.T.), CA156674 (to M.A.T.), CA90571 (to M.A.T.), and S10RR025631 (to P.W.). S.A.H. is a recipient of a USPHS NRSA (GM08496), and M.E.J. and C.J.D. are recipients of a USPHS NRSA (GM07185) from NIH. D.V.D. is the recipient of a postdoctoral fellowship from the United Mitochondrial Disease Foundation and NIH (1F32GM084568). K.S. is a recipient of a CIRM training grant (TG2-01169). P.W. is supported by the Development and Promotion of Science and Technology Talents Project from the Royal Thai Government. D.V.D., S.A.H., M.E.J., C.J.D., K.S., M.A.T., R.D., and C.M.K. designed research; D.V.D., S.A.H., K.S., M.E.J., P.W., and C.J.D. performed research. D.V.D., S.A.H., J.Z., R.D., and C.M.K. contributed to reagents and analytical tools. D.V.D., M.E.J., C.J.D., K.S., M.A.T., and C.M.K. wrote the paper.

Received: May 9, 2011
Revised: January 29, 2013
Accepted: March 6, 2013
Published: April 15, 2013

REFERENCES

Banci, L., Bertini, I., Calderone, V., Cefaro, C., Ciofi-Baffoni, S., Gallo, A., Kallergi, E., Lionaki, E., Pozidis, C., and Tokatlidis, K. (2011). Molecular recognition and substrate mimicry drive the electron-transfer process between MIA40 and ALR. Proc. Natl. Acad. Sci. USA *108*, 4811–4816.

Bernardi, P., and Azzone, G.F. (1981). Cytochrome c as an electron shuttle between the outer and inner mitochondrial membranes. J. Biol. Chem. *256*, 7187–7192.

Bien, M., Longen, S., Wagener, N., Chwalla, I., Herrmann, J.M., and Riemer, J. (2010). Mitochondrial disulfide bond formation is driven by intersubunit electron transfer in Erv1 and proofread by glutathione. Mol. Cell *37*, 516–528.

Bihlmaier, K., Mesecke, N., Terziyska, N., Bien, M., Hell, K., and Herrmann, J.M. (2007). The disulfide relay system of mitochondria is connected to the respiratory chain. J. Cell Biol. *179*, 389–395.

Bourens, M., Dabir, D.V., Tienson, H.L., Sorokina, I., Koehler, C.M., and Barrientos, A. (2012). Role of twin Cys-Xaa9-Cys motif cysteines in mitochondrial import of the cytochrome c oxidase biogenesis factor Cmc1. J. Biol. Chem. *287*, 31258–31269.

Caserta, T.M., Smith, A.N., Gultice, A.D., Reedy, M.A., and Brown, T.L. (2003). Q-VD-OPh, a broad spectrum caspase inhibitor with potent antiapoptotic properties. Apoptosis *8*, 345–352.

Cassidy-Stone, A., Chipuk, J.E., Ingerman, E., Song, C., Yoo, C., Kuwana, T., Kurth, M.J., Shaw, J.T., Hinshaw, J.E., Green, D.R., and Nunnari, J. (2008). Chemical inhibition of the mitochondrial division dynamin reveals its role in Bax/Bak-dependent mitochondrial outer membrane permeabilization. Dev. Cell *14*, 193–204.

Castellano, S., Fiji, H.D., Kinderman, S.S., Watanabe, M., Leon, Pd., Tamanoi, F., and Kwon, O. (2007). Small-molecule inhibitors of protein geranylgeranyltransferase type I. J. Am. Chem. Soc. *129*, 5843–5845.

Cavallaro, G. (2010). Genome-wide analysis of eukaryotic twin CX9C proteins. Mol. Biosyst. *6*, 2459–2470.

Chacinska, A., Pfannschmidt, S., Wiedemann, N., Kozjak, V., Sanjuán Szklarz, L.K., Schulze-Specking, A., Truscott, K.N., Guiard, B., Meisinger, C., and Pfanner, N. (2004). Essential role of Mia40 in import and assembly of mitochondrial intermembrane space proteins. EMBO J. *23*, 3735–3746.

Chacinska, A., Guiard, B., Müller, J.M., Schulze-Specking, A., Gabriel, K., Kutik, S., and Pfanner, N. (2008). Mitochondrial biogenesis, switching the sorting pathway of the intermembrane space receptor Mia40. J. Biol. Chem. *283*, 29723–29729.

Chacinska, A., Koehler, C.M., Milenkovic, D., Lithgow, T., and Pfanner, N. (2009). Importing mitochondrial proteins: machineries and mechanisms. Cell *138*, 628–644.

Claypool, S.M., Oktay, Y., Boontheung, P., Loo, J.A., and Koehler, C.M. (2008). Cardiolipin defines the interactome of the major ADP/ATP carrier protein of the mitochondrial inner membrane. J. Cell Biol. *182*, 937–950.

Crugeiras, J., Rios, A., Riveiros, E., and Richard, J.P. (2009). Substituent effects on the thermodynamic stability of imines formed from glycine and aromatic aldehydes: implications for the catalytic activity of pyridoxal-5′-phosphate. J. Am. Chem. Soc. *131*, 15815–15824.

Curado, S., Ober, E.A., Walsh, S., Cortes-Hernandez, P., Verkade, H., Koehler, C.M., and Stainier, D.Y. (2010). The mitochondrial import gene tomm22 is

specifically required for hepatocyte survival and provides a liver regeneration model. Dis. Model. Mech. *3*, 486–495.

Curran, S.P., Leuenberger, D., Oppliger, W., and Koehler, C.M. (2002). The Tim9p-Tim10p complex binds to the transmembrane domains of the ADP/ATP carrier. EMBO J. *21*, 942–953.

Curran, S.P., Leuenberger, D., Leverich, E.P., Hwang, D.K., Beverly, K.N., and Koehler, C.M. (2004). The role of Hot13p and redox chemistry in the mitochondrial TIM22 import pathway. J. Biol. Chem. *279*, 43744–43751.

Dabir, D.V., Leverich, E.P., Kim, S.K., Tsai, F.D., Hirasawa, M., Knaff, D.B., and Koehler, C.M. (2007). A role for cytochrome c and cytochrome c peroxidase in electron shuttling from Erv1. EMBO J. *26*, 4801–4811.

Deponte, M., and Hell, K. (2009). Disulphide bond formation in the intermembrane space of mitochondria. J. Biochem. *146*, 599–608.

Di Fonzo, A., Ronchi, D., Lodi, T., Fassone, E., Tigano, M., Lamperti, C., Corti, S., Bordoni, A., Fortunato, F., Nizzardo, M., et al. (2009). The mitochondrial disulfide relay system protein GFER is mutated in autosomal-recessive myopathy with cataract and combined respiratory-chain deficiency. Am. J. Hum. Genet. *84*, 594–604.

Doorn, J.A., and Petersen, D.R. (2003). Covalent adduction of nucleophilic amino acids by 4-hydroxynonenal and 4-oxononenal. Chem. Biol. Interact. *143-144*, 93–100.

Duncan, M.C., Ho, D.G., Huang, J., Jung, M.E., and Payne, G.S. (2007). Composite synthetic lethal identification of membrane traffic inhibitors. Proc. Natl. Acad. Sci. USA *104*, 6235–6240.

Farrell, S.R., and Thorpe, C. (2005). Augmenter of liver regeneration: a flavin-dependent sulfhydryl oxidase with cytochrome c reductase activity. Biochemistry *44*, 1532–1541.

Gerber, J., Mühlenhoff, U., Hofhaus, G., Lill, R., and Lisowsky, T. (2001). Yeast ERV2p is the first microsomal FAD-linked sulfhydryl oxidase of the Erv1p/Alrp protein family. J. Biol. Chem. *276*, 23486–23491.

Gross, E., Sevier, C.S., Vala, A., Kaiser, C.A., and Fass, D. (2002). A new FAD-binding fold and intersubunit disulfide shuttle in the thiol oxidase Erv2p. Nat. Struct. Biol. *9*, 61–67.

Hasson, S.A., Damoiseaux, R., Glavin, J.D., Dabir, D.V., Walker, S.S., and Koehler, C.M. (2010). Substrate specificity of the TIM22 mitochondrial import pathway revealed with small molecule inhibitor of protein translocation. Proc. Natl. Acad. Sci. USA *107*, 9578–9583.

Herrmann, J.M., and Hell, K. (2005). Chopped, trapped or tacked—protein translocation into the IMS of mitochondria. Trends Biochem. Sci. *30*, 205–211.

Hofmann, S., Rothbauer, U., Mühlenbein, N., Baiker, K., Hell, K., and Bauer, M.F. (2005). Functional and mutational characterization of human MIA40 acting during import into the mitochondrial intermembrane space. J. Mol. Biol. *353*, 517–528.

Horn, D., Al-Ali, H., and Barrientos, A. (2008). Cmc1p is a conserved mitochondrial twin CX9C protein involved in cytochrome c oxidase biogenesis. Mol. Cell. Biol. *28*, 4354–4364.

Ivanova, N.B., Dimos, J.T., Schaniel, C., Hackney, J.A., Moore, K.A., and Lemischka, I.R. (2002). A stem cell molecular signature. Science *298*, 601–604.

Kirdant, A.S., Shelke, V.A., Shankarwar, S.G., Shankarwar, A.G., and Chondhekar, T.K. (2011). Kinetic study of hydrolysis of N-salicylidene-m-methyl aniline spectrophotometrically. J. Chem. Pharm. Res. *3*, 790–796.

Koehler, C.M., and Tienson, H.L. (2009). Redox regulation of protein folding in the mitochondrial intermembrane space. Biochim. Biophys. Acta *1793*, 139–145.

Lange, H., Lisowsky, T., Gerber, J., Mühlenhoff, U., Kispal, G., and Lill, R. (2001). An essential function of the mitochondrial sulfhydryl oxidase Erv1p/ALR in the maturation of cytosolic Fe/S proteins. EMBO Rep. *2*, 715–720.

Lumsden, A.L., Henshall, T.L., Dayan, S., Lardelli, M.T., and Richards, R.I. (2007). Huntingtin-deficient zebrafish exhibit defects in iron utilization and development. Hum. Mol. Genet. *16*, 1905–1920.

McClure, K.D., Sustar, A., and Schubiger, G. (2008). Three genes control the timing, the site and the size of blastema formation in Drosophila. Dev. Biol. *319*, 68–77.

Mendelsohn, B.A., Yin, C., Johnson, S.L., Wilm, T.P., Solnica-Krezel, L., and Gitlin, J.D. (2006). Atp7a determines a hierarchy of copper metabolism essential for notochord development. Cell Metab. *4*, 155–162.

Mesecke, N., Terziyska, N., Kozany, C., Baumann, F., Neupert, W., Hell, K., and Herrmann, J.M. (2005). A disulfide relay system in the intermembrane space of mitochondria that mediates protein import. Cell *121*, 1059–1069.

Milenkovic, D., Ramming, T., Müller, J.M., Wenz, L.S., Gebert, N., Schulze-Specking, A., Stojanovski, D., Rospert, S., and Chacinska, A. (2009). Identification of the signal directing Tim9 and Tim10 into the intermembrane space of mitochondria. Mol. Biol. Cell *20*, 2530–2539.

Mochizuki, Y., and Furukawa, K. (1987). Application of coomassie brilliant blue staining to cultured hepatocytes. Cell Biol. Int. Rep. *11*, 367–371.

Mokranjac, D., and Neupert, W. (2009). Thirty years of protein translocation into mitochondria: unexpectedly complex and still puzzling. Biochim. Biophys. Acta *1793*, 33–41.

Murphey, R.D., and Zon, L.I. (2006). Small molecule screening in the zebrafish. Methods *39*, 255–261.

Nordfelth, R., Kauppi, A.M., Norberg, H.A., Wolf-Watz, H., and Elofsson, M. (2005). Small-molecule inhibitors specifically targeting type III secretion. Infect. Immun. *73*, 3104–3114.

Parone, P.A., James, D.I., Da Cruz, S., Mattenberger, Y., Donzé, O., Barja, F., and Martinou, J.C. (2006). Inhibiting the mitochondrial fission machinery does not prevent Bax/Bak-dependent apoptosis. Mol. Cell. Biol. *26*, 7397–7408.

Ramalho-Santos, M., Yoon, S., Matsuzaki, Y., Mulligan, R.C., and Melton, D.A. (2002). "Stemness": transcriptional profiling of embryonic and adult stem cells. Science *298*, 597–600.

Riemer, J., Fischer, M., and Herrmann, J.M. (2011). Oxidation-driven protein import into mitochondria: Insights and blind spots. Biochim. Biophys. Acta *1808*, 981–989.

Rissler, M., Wiedemann, N., Pfannschmidt, S., Gabriel, K., Guiard, B., Pfanner, N., and Chacinska, A. (2005). The essential mitochondrial protein Erv1 cooperates with Mia40 in biogenesis of intermembrane space proteins. J. Mol. Biol. *353*, 485–492.

Ryan, M.T., Müller, H., and Pfanner, N. (1999). Functional staging of ADP/ATP carrier translocation across the outer mitochondrial membrane. J. Biol. Chem. *274*, 20619–20627.

Scorrano, L., Ashiya, M., Buttle, K., Weiler, S., Oakes, S.A., Mannella, C.A., and Korsmeyer, S.J. (2002). A distinct pathway remodels mitochondrial cristae and mobilizes cytochrome c during apoptosis. Dev. Cell *2*, 55–67.

Senkevich, T.G., White, C.L., Koonin, E.V., and Moss, B. (2002). Complete pathway for protein disulfide bond formation encoded by poxviruses. Proc. Natl. Acad. Sci. USA *99*, 6667–6672.

Shamblott, M.J., Axelman, J., Wang, S., Bugg, E.M., Littlefield, J.W., Donovan, P.J., Blumenthal, P.D., Huggins, G.R., and Gearhart, J.D. (1998). Derivation of pluripotent stem cells from cultured human primordial germ cells. Proc. Natl. Acad. Sci. USA *95*, 13726–13731.

Shaw, G.C., Cope, J.J., Li, L., Corson, K., Hersey, C., Ackermann, G.E., Gwynn, B., Lambert, A.J., Wingert, R.A., Traver, D., et al. (2006). Mitoferrin is essential for erythroid iron assimilation. Nature *440*, 96–100.

Shu, X., Huang, J., Dong, Y., Choi, J., Langenbacher, A., and Chen, J.N. (2007). Na,K-ATPase alpha2 and Ncx4a regulate zebrafish left-right patterning. Development *134*, 1921–1930.

Sideris, D.P., and Tokatlidis, K. (2010). Oxidative protein folding in the mitochondrial intermembrane space. Antioxid. Redox Signal. *13*, 1189–1204.

Sideris, D.P., Petrakis, N., Katrakili, N., Mikropoulou, D., Gallo, A., Ciofi-Baffoni, S., Banci, L., Bertini, I., and Tokatlidis, K. (2009). A novel intermembrane space-targeting signal docks cysteines onto Mia40 during mitochondrial oxidative folding. J. Cell Biol. *187*, 1007–1022.

Stojanovski, D., Milenkovic, D., Müller, J.M., Gabriel, K., Schulze-Specking, A., Baker, M.J., Ryan, M.T., Guiard, B., Pfanner, N., and Chacinska, A. (2008). Mitochondrial protein import: precursor oxidation in a ternary complex with disulfide carrier and sulfhydryl oxidase. J. Cell Biol. *183*, 195–202.

Tang, C., Lee, A.S., Volkmer, J.P., Sahoo, D., Nag, D., Mosley, A.R., Inlay, M.A., Ardehali, R., Chavez, S.L., Pera, R.R., et al. (2011). An antibody against

SSEA-5 glycan on human pluripotent stem cells enables removal of teratoma-forming cells. Nat. Biotechnol. *29*, 829–834.

Terziyska, N., Grumbt, B., Bien, M., Neupert, W., Herrmann, J.M., and Hell, K. (2007). The sulfhydryl oxidase Erv1 is a substrate of the Mia40-dependent protein translocation pathway. FEBS Lett. *581*, 1098–1102.

Terziyska, N., Grumbt, B., Kozany, C., and Hell, K. (2009). Structural and functional roles of the conserved cysteine residues of the redox-regulated import receptor Mia40 in the intermembrane space of mitochondria. J. Biol. Chem. *284*, 1353–1363.

Thorpe, C., Hoober, K.L., Raje, S., Glynn, N.M., Burnside, J., Turi, G.K., and Coppock, D.L. (2002). Sulfhydryl oxidases: emerging catalysts of protein disulfide bond formation in eukaryotes. Arch. Biochem. Biophys. *405*, 1–12.

Tienson, H.L., Dabir, D.V., Neal, S.E., Loo, R., Hasson, S.A., Boontheung, P., Kim, S.K., Loo, J.A., and Koehler, C.M. (2009). Reconstitution of the mia40-erv1 oxidative folding pathway for the small tim proteins. Mol. Biol. Cell *20*, 3481–3490.

Todd, L.R., Damin, M.N., Gomathinayagam, R., Horn, S.R., Means, A.R., and Sankar, U. (2010a). Growth factor erv1-like modulates Drp1 to preserve mitochondrial dynamics and function in mouse embryonic stem cells. Mol. Biol. Cell *21*, 1225–1236.

Todd, L.R., Gomathinayagam, R., and Sankar, U. (2010b). A novel Gfer-Drp1 link in preserving mitochondrial dynamics and function in pluripotent stem cells. Autophagy *6*, 821–822.

Truscott, K.N., Wiedemann, N., Rehling, P., Müller, H., Meisinger, C., Pfanner, N., and Guiard, B. (2002). Mitochondrial import of the ADP/ATP carrier: the essential TIM complex of the intermembrane space is required for precursor release from the TOM complex. Mol. Cell. Biol. *22*, 7780–7789.

Vitu, E., Bentzur, M., Lisowsky, T., Kaiser, C.A., and Fass, D. (2006). Gain of function in an ERV/ALR sulfhydryl oxidase by molecular engineering of the shuttle disulfide. J. Mol. Biol. *362*, 89–101.

Volkmann, K., Lucas, J.L., Vuga, D., Wang, X., Brumm, D., Stiles, C., Kriebel, D., Der-Sarkissian, A., Krishnan, K., Schweitzer, C., et al. (2011). Potent and selective inhibitors of the inositol-requiring enzyme 1 endoribonuclease. J. Biol. Chem. *286*, 12743–12755.

Waterhouse, N.J., Goldstein, J.C., Kluck, R.M., Newmeyer, D.D., and Green, D.R. (2001). The (Holey) study of mitochondria in apoptosis. Methods Cell Biol. *66*, 365–391.

Webb, T.R. (2005). Current directions in the evolution of compound libraries. Curr. Opin. Drug Discov. Devel. *8*, 303–308.

Wingert, R.A., Galloway, J.L., Barut, B., Foott, H., Fraenkel, P., Axe, J.L., Weber, G.J., Dooley, K., Davidson, A.J., Schmid, B., et al.; Tübingen 2000 Screen Consortium. (2005). Deficiency of glutaredoxin 5 reveals Fe-S clusters are required for vertebrate haem synthesis. Nature *436*, 1035–1039.

Wu, C.K., Dailey, T.A., Dailey, H.A., Wang, B.C., and Rose, J.P. (2003). The crystal structure of augmenter of liver regeneration: A mammalian FAD-dependent sulfhydryl oxidase. Protein Sci. *12*, 1109–1118.

Yamagata, K., Daiho, T., and Kanazawa, T. (1993). Labeling of lysine 492 with pyridoxal 5′-phosphate in the sarcoplasmic reticulum Ca(2+)-ATPase. Lysine 492 residue is located outside the fluorescein 5-isothiocyanate-binding region in or near the ATP binding site. J. Biol. Chem. *268*, 20930–20936.

Zhang, J., Khvorostov, I., Hong, J.S., Oktay, Y., Vergnes, L., Nuebel, E., Wahjudi, P.N., Setoguchi, K., Wang, G., Do, A., et al. (2011). UCP2 regulates energy metabolism and differentiation potential of human pluripotent stem cells. EMBO J. *30*, 4860–4873.